Materials Research Express

PAPER • **OPEN ACCESS**

The effect of synthesis temperature on the properties of TiO_2 (B) nanorods and its precursors as anode materials for lithium-ion batteries

To cite this article: Ntombizodwa M Ncube and Haitao Zheng 2020 *Mater. Res. Express* **7** 015504

Materials Research Express

OPEN ACCESS

RECEIVED
29 October 2019

REVISED
4 December 2019

ACCEPTED FOR PUBLICATION
13 December 2019

PUBLISHED
6 January 2020

PAPER

The effect of synthesis temperature on the properties of TiO_2 (B) nanorods and its precursors as anode materials for lithium-ion batteries

Ntombizodwa M Ncube and Haitao Zheng

Energy Centre, Council for Scientific and Industrial Research (CSIR), PO Box 395, Pretoria, 0001, South Africa

E-mail: hzheng@csir.co.za

Keywords: hydrogen titanate, TiO_2(B), nanorods, anode, lithium ion battery

Abstract

In this work, we carried out a detailed research on the effect of synthesis temperature on the properties of TiO_2 (B) nanorods and its hydrogen titanate precursors. At the initial stage, hydrogen titanates (HTOs) were synthesised at different temperatures (140 °C–180 °C). The HTO materials were then annealed at 400 °C for 2 h in the second-stage to produce TiO_2 (B) nanorods. It is interesting to note that the pure anatase phase of TiO_2 nanorods (TO140) was achieved from the HTO material (HTO140) prepared at 140 °C, while the TiO_2 (B) nanorods were only formed from those synthesised at 160 °C (HTO160) and 180 °C (HTO180). In the evaluation of these materials as anodes for lithium ion batteries (LIBs), HTO140 showed better rate performance at higher current rates (500–1000 mAg^{-1}). However, HTO160 and HTO180 displayed lower initial discharge capacities than that of their precursor (the commercial TO) at 200 mAg^{-1}. Addtionally, HTO160 exhibited the best stability with 71.5% retention after 100 cycles at 200 mAg^{-1}. Moreover, the annealed product of TO140 from HTO140 demonstrated the highest initial discharge capacity with a value of 164.3 $mAhg^{-1}$ at a current of 200 mAg^{-1}, which is corresponding to its low charge transfer resistance. However, TO160 showed a superior stability with 92.3% retained capacity after 100 cycles at 200 mAg^{-1}. Overall, 160 °C is the optimum temperature to synthesize TiO_2 (B) nanorods, regarding to its good cycling stability and mild capacity as anode materials. The investigation showed that the synthesis temperature is a determining factor to producing either TiO_2 (B) or anatase TiO_2 nanorods, has an influence on the properties of the precursor as well as the TiO_2 (B) as anode materials for LIBs.

1. Introduction

Many efforts have been made over the years to find alternative anode materials for applications in lithium-ion batteries (LIBs) with high energy and power. The anode materials, such as Si [1–3], Sn [4, 5], Sb [6, 7], Al [8], CuO [9, 10], MoO_3 [11], Co_3O_4 [12], MnO_3 [13] and WO_3 [14] have been investigated and were found to be attractive with high capacities ranging from 200–4200 mAh g^{-1} [1, 8, 11, 14–21]. However, most of these high capacity materials, including graphite suffers from large volume expansion (300%–400%) due to low operating voltages (0–0.05 V), which causes pulverization of the materials and results in rapid capacity decay [8, 22, 23]. This effect promotes the decomposition of most organic electrolytes, which leads to pressure build due to release of gases and highly endangers the safety of the battery. Alternatively, Titanium-based oxides mainly referred to as lithium titanate $Li_4Ti_5O_{12}$ (LTO) and titanium dioxide (TiO_2), have been considered as the next-generation potential graphite substitutes anode materials. In fact, LTO is commercially available as an alternative or possible replacement of graphite for lithium–ion batteries. However, the LTO has a low theoretical capacity of 175 mAh g^{-1}, a poor electronic and lithium ionic conductivities which limit its high-rate capability [24–27]. Alternatively, the theoretical capacity of TiO_2 is 335 mAh g^{-1} that is gravimetrically comparable with the commercialized graphite (372 mAh g^{-1}) [28] . In addition, it operates at a relatively high voltage (1.5–1.8 V versus Li/Li^+) where most organic electrolytes are thermally stable [21]. TiO_2 affords LIBs safety with a volume

change of <3% during insertion of Li-ions, which makes this material of exceptional value [29]. The latter is considered the most important requirement for LIBs, especially for stationary energy storage purposes [23]. It is also an abundant resource with relatively low costs, environmentally friendly and chemically stable [23, 29–31]. Unfortunately, TiO_2 is associated with conductivity and ion transport limitations during cycling, which makes it a poor electrical conductor with low diffusion coefficient of the Li-ions [32]. Moreover, TiO_2 has low specific capacity of 160 mAh g^{-1}. Some approaches were explored to increase specific capacity of TiO_2 to reach theoretical capacity, including restructure, composited with other materials, carbon coating and ion doping [13, 33, 34]. Among these, the nanostructured materials, including nanowires, nanotubes, nanosheets, nanorods and nanofibres have afforded some advantages, improving the capacity, cycle life and rate capability. Although, the larger surface area of the nanostructured materials reduces the diffusion length, the many active sites allow uncontrollable external reactions to occur, which would result in biased overall performance of the material [34, 35]. Besides three natural polymorphs of tetragonal anatase, tetragonal rutile, and orthorhombic brookite phases, TiO_2-bronze (B) phase has attracted great attention due to its unique monoclinic structure with fibrous morphology. It possesses a relatively lower density/ higher volume than that of the three popular phases of the anatase, rutile, or brookite [36].

In this work, we report on the hydrothermally synthesized TiO_2 (B) under different temperatures. Additionally, the effects of thermal treatment on the morphology and electrochemical performance of the materials are explored. Moreover, a comparison study of the battery performances are carried out between the precursors (hydrogen titanates) and TiO_2 (B) nanorods through thermal treatment.

2. Experimental section

2.1. Synthesis of TiO_2 nanorods

TiO_2 (P25, Degussa, Germany) powder was washed with deionised water to remove impurities prior to the synthesis. A two-step synthesis procedure was followed to produce TiO_2 nanorods from the preliminary product, hydrogen titanate (HTO) materials using the hydrothermal method [37]. In the first step, TiO_2 powder was mixed with 150 ml of 10 M NaOH aqueous solution. After stirring for 2 h the suspensions were transferred into a Teflon-lined autoclave and heated at different temperatures (140, 160 and 180 °C) for 48 h with continuous stirring. The products were filtered, acid-washed with 0.1 M HCl, filtered again and finally washed with distilled water to a neutral pH and dried at 110 °C overnight. The products were marked as HTO140, HTO160 and HTO180, respectively. The samples were then annealed in the second-step using a tube furnace at 400 °C for 2 h under air to obtain TiO_2 (B) nanorods labelled as TO140, TO160 and TO180, respectively.

2.2. Materials characterization

The resultant powders were characterized by an x-ray diffractometer (Rigaku, Japan) using a CuK_α radiation with $\lambda = 0.1545$ nm at 45 kV and 40 mA. The morphology of the materials was determined by the field emission scanning microscope (FE-SEM, Joel JSM-7500F, Tokyo, Japan). An ink was made from the active material, carbon black and binder with ratio of 80:10:10, respectively in *N*-methyl-pyrrolidone (NMP). The ink was uniformly spread on a copper foil using a doctor blade and dried in a vacuum oven at 110 °C overnight. The electrochemical coin cells (CR 2032) were assembled in an argon filled glove box with oxygen (O_2) and moisture (H_2O) contents less than 10 ppm. The HTO and TO as the working electrodes, while Li metal was used as both the reference and counter electrodes. Celgard porous propylene film as the separator and 1 M $LiPF_6$ dissolved in a 1:1:1 ratio mixture of ethylene carbonate (EC)/diethyl carbonate (DEC)/dimethyl carbonate (DMC) was used as the electrolyte. The assembled coin cells were aged for 24 h prior the electrochemical measurements. The MACCOR battery tester (series 4000, Tusla, USA) was used for testing battery performance. The mass of the active material was used to calculate the current density and the specific capacity. The electrochemical impedance spectrometry (EIS) and cycle voltammetry (CV) experiments were carried out using a Bio-Logic science VMP3-based instrument.

3. Results and discussion

3.1. SEM images

The SEM images in figure 1 depict the morphology of the as-synthesised materials, HTO140, HTO160, HTO180, and TO160 and the commercial TO. The commercial TO shows nanoparticles in the range 40–60 nm and were converted to HTO nanorods (figures 1(b)–(d)) after the hydrothermal treatment. With increasing temperature, more HTO layers were formed and became longer, as shown in figures 1(b)–(d). For comparison, the SEM image of TO160 in figure 1(e) shows rods through edging differences compared with the layered HTO160 (figure 1(c)), although both materials have similar sizes and shapes.

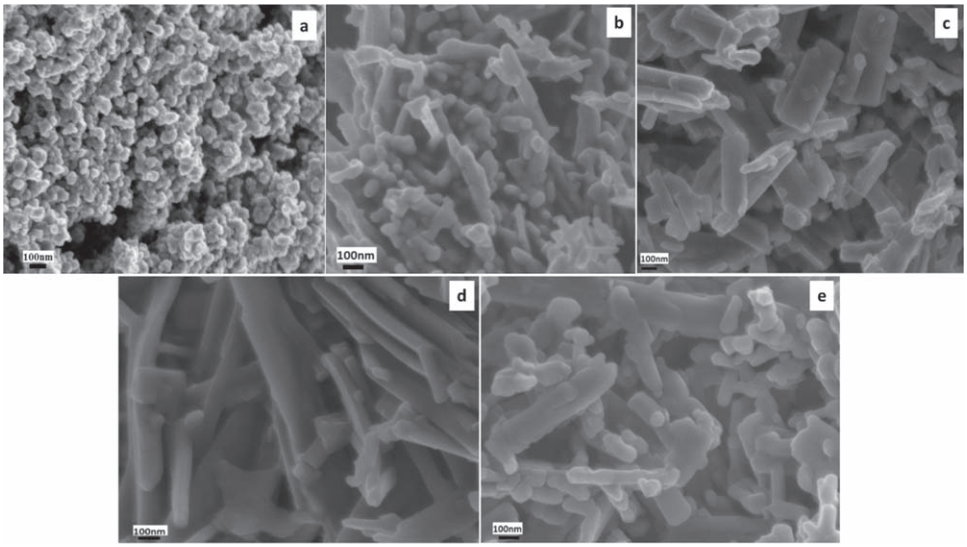

Figure 1. FE-SEM images of the commercial TO (a); HTO140 (b); HTO160 (c); HTO180 (d) and TO160 (e) materials.

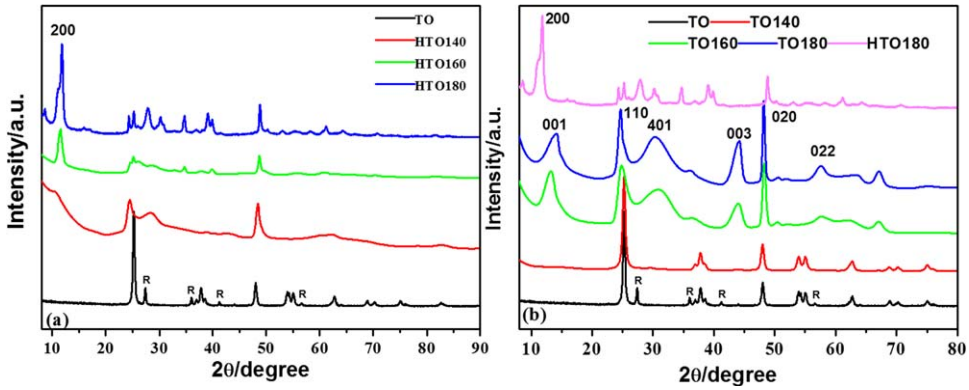

Figure 2. XRD patterns of the commercial TO, HTO and TO materials.

3.2. XRD analysis

The XRD patterns of the as prepared HTO, TO materials and the commercial TO are depicted in figure 2. All the observed diffraction patterns of the commercial TO in figure 2(a) were consistent with the crystal structure of anatase (JCPDS-21–1272) with impurity traits of rutile marked R [38]. The HTO140, HTO160 and HTO180 powders (figure 2(a)), can be identified as mixtures of $H_2Ti_3O_7$ and $H_xTi_{2-x/4\times-2}O_4(x = 0.75)$ with typical plane of [200] located in $\sim 10^0$ [39]. With increasing temperature, the peak of the [200] plane increased also, indicating the improved crystallinity of HTO. Figure 2(b) shows the XRD of TO nanorods from HTO materials and commercial TO. It is interesting that HTO140 converted to the pure anatase phase (TO140) without rutile impurities. TO160 and TO180 materials were corresponding to the monoclinic TiO_2 (B) phase with typical planes of [110], [110], [401], [003], [020] and [022] [40, 41]. The formation of the phases can be explained from the following mechanism during the synthesis process on mixing TO powder with NaOH solution at high temperatures, the Ti–O–Ti bond might cleave to form a mixture of layered sodium titanate (Ti–O–Na). The lamellar sheets will then form due to the electrostatic repulsion of the charge on the Na. Acid wash with HCl causes an ion exchange between the Na^+ and H^+ to obtain the HTO [40, 41]. Therefore, it is only after calcination of HTO that the loss of water gives TO as the resultant product. However, it is evident that only TO140 was able to convert to pure anatase TO phase, while TO160 and TO180 exhibited the monoclinic TiO_2 (B) structure. This is suspected to be due to hindrances within the crystal structure for proper roll up of the lamellar sheets into rods influenced by the effects of temperature during the synthesis [40]. Previous studies reported that temperatures greater than 150 °C during the synthesis are prone to destruct the roll up of the lamellar sheets due to granular particles from agglomerations and this decreases the surface area and pore size [40, 41].

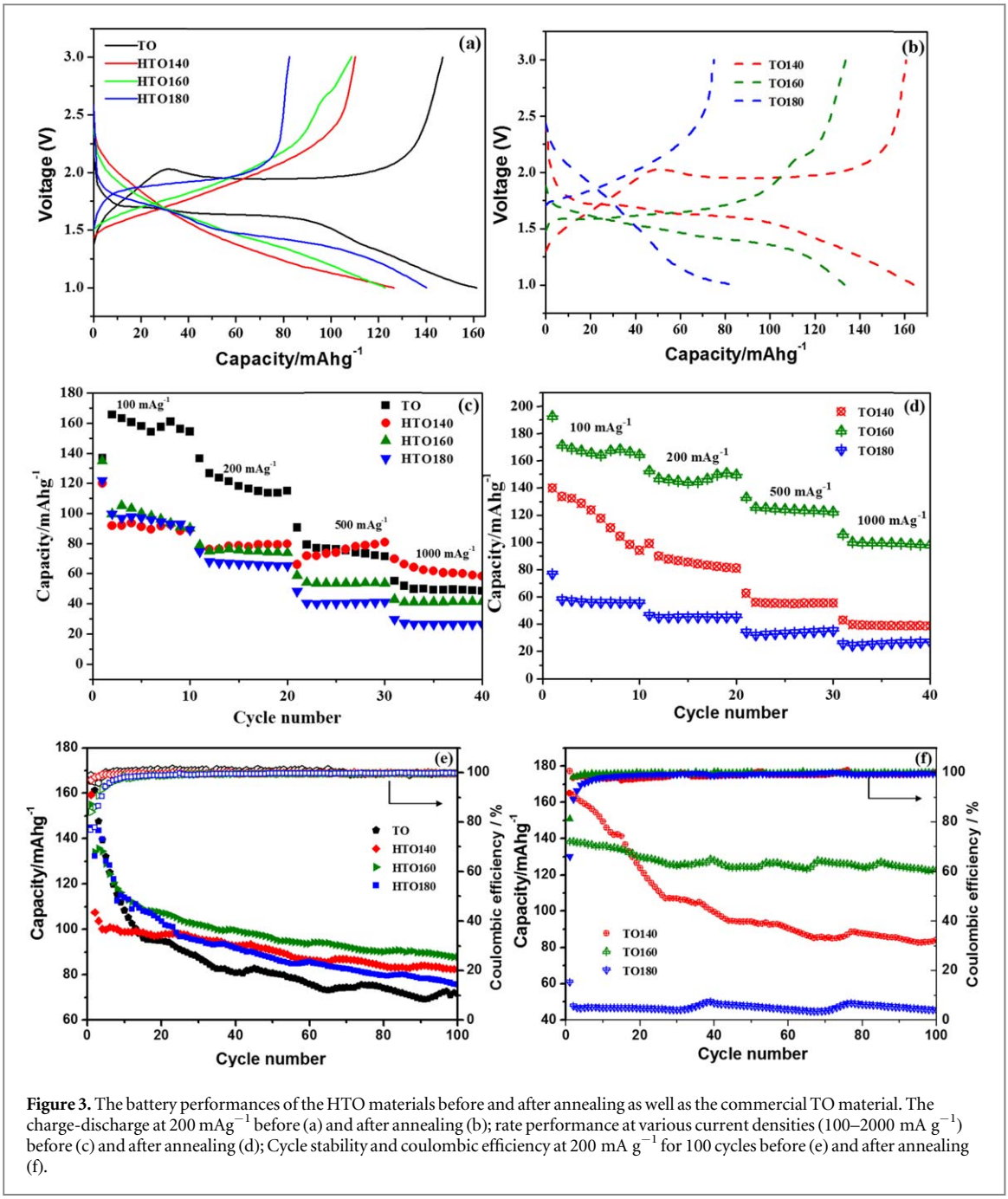

Figure 3. The battery performances of the HTO materials before and after annealing as well as the commercial TO material. The charge-discharge at 200 mAg^{-1} before (a) and after annealing (b); rate performance at various current densities (100–2000 mA g^{-1}) before (c) and after annealing (d); Cycle stability and coulombic efficiency at 200 mA g^{-1} for 100 cycles before (e) and after annealing (f).

3.3. Battery performance

The battery behaviours of the HTO before and after annealing as well as the commercial TO materials are shown in figure 3 and table 1. The discharge/charge profiles in figures 3(a), (b) displays similar behaviours with the HTO nanosheets without platform [42].

The HTO materials delivered capacities in the range of 122.9–140.2 $mAhg^{-1}$ at 200 mAg^{-1} as illustrated in figure 3(a) and table 1, which are lower than that of 161.3 $mAhg^{-1}$ of the commercial TO nanoparticles. The order of capacity decrease was the commercial TO (160 $mAhg^{-1}$) > HTO180 (140.2 $mAhg^{-1}$) > HTO140 (126.5 $mAhg^{-1}$) > HTO160 (122.9 $mAhg^{-1}$). After annealing, TO140 showed an improved capacity and better reversibility compared to HTO140 in figure 3(b). TO160 maintained a similar capacity with HTO160. However, the capacity of TO180 worsened compared to it precursor of the HTO180.

To further evaluate the battery performance, the rate performances were plotted in figures 3(e), (f) at various current densities (100–1000 mAg^{-1}) for HTO, TO and commercial TO materials. Generally, the rate performance shows the relation between capacity and increasing current density. In addition, the retained capacity corresponds to the stability of the material. It can be seen in figure 3(e) that the discharge capacity of the commercial TO material is highest in the lower current density (100–200 mAg^{-1}) among the other materials. However, the HTO140 shows the best capacity in the current range of 500–1000 mAg^{-1}. The HTO180 capacity

Table 1. Summarised data from the battery performances of the HTO before/after annealing and the commercial TO material.

Samples	Capacity ($mAhg^{-1}$) at 2st cycle	Capacity ($mAhg^{-1}$) at 100 cycles	Retention (%)
TO	161.3	71.7	44.4
HTO140	126.5	82.2	65
HTO160	122.9	87.9	**71.5**
HTO180	140.2	75.6	53.9
TO140	164.3	84.2	51.2
TO160	133.4	123.1	**92.3**
TO180	84.1	45.4	54

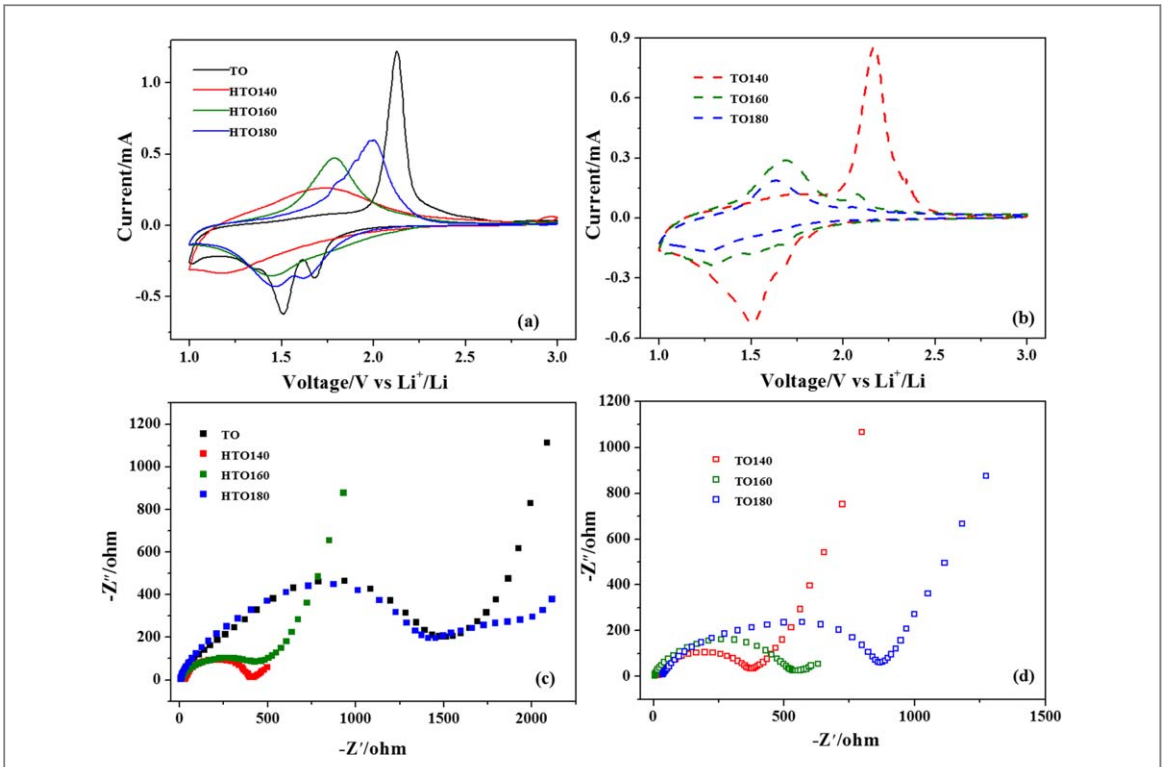

Figure 4. CV curves of HTO (a) and TO (b) electrodes at a scan rate of 0.1 mV s^{-1} between 1.0 and 3.0 V and Nyquist plots of the HTO (c) and TO electrodes (d) in the frequency range of 100 kHz−10 mHz.

decreased drastically when the current increased. After annealing, TO160 shows the best performance in the full range of current, followed by TO140 and TO180 as depicted in figure 3(f). The cycling performances of the commercial TO and the HTO materials were also tested before and after annealing at 200 mAg^{-1} for 100 cycles as displayed in figures 3(e), (f). Before annealing, HTO160 had the best stability with 71.5% retained capacity after 100 cycles, followed by HTO140 (65.0%), HTO180 (53.9%) and TO (44.4%), which is in agreement with the rate performances of figure 3(c). After annealing, the TO materials displayed the same order with the HTO materials, TO160 had the best stability with 92.3% retention, which matches with the rate performance displayed in figure 3(d). The coulombic efficiency of the materials were compared in figures 3 (e), (f). It is observed that all the materials show low initial efficiency and after few cycles remain above 99% through 100 cycles.

3.4. Electrochemical behaviour

Figure 4 displays cycle voltammetry (CV) and electrochemical impedance spectrometry (EIS). To understand the ionic diffusion process and phase transformation during the electrode reactions, the CV curves were conducted in the potential range of 1.0 ∼ 3.0 V at a scan rate of 0.1 mV s^{-1} as shown in figure 4(a), (b). The anodic peaks of the HTO materials in figure 4(a) were more negative and wide compared with the commercial TO material. The pair of peaks on the HTO materials are ascribed to the pseudocapacitive lithium storage behaviour, while the pair of the commercial TO at 1.5 (1.7)/2.1 V are assigned to the solid-state lithium diffusion

into TiO_2, which are consistent with previously reported data [43–45]. The TO electrode has two cathodic peaks due to impurities. By comparing the CV curves of the TO electrode with that of the HTO, the gap between the redox peaks of the latter are smaller, indicating a lower electrode polarization and a higher lithium-ion diffusivity.

The CV curves of the HTO materials after annealing are shown in figure 4(b). Compared with the TO160 and TO180, it was observed that the shapes of redox peak on the TO140 electrode at 1.5/2.2 V are sharper and intense, which is similar to the commercial TO due to the pure anatase phase of the TO140. It is notable that the TO160 shows two pairs of peaks at 1.3/1.7 V and 1.7/2.1 V, which are a match with the pseudocapacitive process and lithium intercalation of TiO_2 (B). The gap between the redox peaks of the TO160 and TO180 are smaller than that of the TO140. The phenomenon confirms that the HTO with/without annealing are beneficial to intercalation/deintercalation of lithium.

Figures 4(c), (d) shows the Nyquist plot for both the HTO and TO electrodes. All the Nyquist plots are defined by a semicircle at high frequencies and a straight line at low frequencies, corresponding to the charge transfer (R_{ct}) and diffusion of Li ions, respectively [46]. The R_{ct} values of the HTO140, HTO160 and HTO180 are 383.4, 422.3 and 1412.5 Ω, respectively, which are lower than the 1470.3 Ω of the TO. After annealing, the increasing order of R_{ct} value is TO140 (362.5 Ω) $<$ TO160 (520.3 Ω) $<$ TO180 (832.1 Ω). Overall, the prepared HTO materials before/after annealing have shown better charge transfer than the commercial TO.

4. Conclusions

A series of hydrogen titanates (HTOs) were synthesised at 140, 160, and 180 °C using the hydrothermal method. TiO_2 nanorods were obtained after annealing of the HTO at 400 °C for 2 h. HTO140 converted to the pure anatase TiO_2 nanorods (TO140). While HTO160 and HTO180, synthesised above 140 °C formed TiO_2 (B) nanorods. The HTO and the TO materials battery performances were explored as promising anode materials. The HTO materials displayed lower initial discharge capacity (~123–~140 $mAhg^{-1}$) than that of their precursor (~160 $mAhg^{-1}$) at a current of 200 mAg^{-1}. However, the HTO140 showed better rate performance than that of the precursor in the higher rates. Moreover, the HTO160 exhibited best stability with 71.5% retention after 100 cycles at 200 mAg^{-1}. After annealing of the HTO materials, the TO140 material demonstrated the highest initial discharge capacity. However, TO160 showed superior stability with 92.3% retained capacity after 100 cycles at 200 mAg^{-1}.

Acknowledgments

The authors are thankful for the financial support from the CSIR.

ORCID iDs

Haitao Zheng https://orcid.org/0000-0003-4180-0197

References

[1] Winter M, Besenhard J O, Spahr M E and Novák P 1998 Insertion electrode materials for rechargeable lithium batteries *Adv. Mater.* **10** 725–63
[2] Hansen S, Quiroga-González E, Carstensen J and Föll H 2016 Size-dependent cyclic voltammetry study of silicon microwire anodes for lithium ion batteries *Electrochim. Acta* **217** 283–91
[3] Byrd I and Wu J 2016 Asymmetric membranes containing micron-size silicon for high performance lithium ion battery anode *Electrochim. Acta* **213** 46–54
[4] Javadian S, Kakemam J, Sadeghi A and Gharibi H 2016 Pulsed current electrodeposition parameters to control the sn particle size to enhance electrochemical performance as anode material in lithium ion batteries *Surf. Coat. Technol.* **305** 41–8
[5] Schmuelling G *et al* 2016 Synthesis and electrochemical characterization of nano-sized ag 4 sn particles as anode material for lithium-ion batteries *Electrochim. Acta* **196** 597–602
[6] Lakshmi D and Nalini B 2017 Performance of SnSb: Ce, co alloy as anode for lithium-ion batteries *J. Solid State Electrochem.* **21** 1027–34
[7] Yi Z, Han Q, Zan P, Wu Y, Cheng Y and Wang L 2016 Sb nanoparticles encapsulated into porous carbon matrixes for high-performance lithium-ion battery anodes *J. Power Sources* **331** 16–21
[8] Sharma S, Kim M, Kim D and Yu J 2013 Al nanorod thin films as anode electrode for li ion rechargeable batteries *Electrochim. Acta* **87** 872–9
[9] Cheng S *et al* 2016 *In-situ* oxidized copper-based hybrid film on carbon cloth as flexible anode for high performance lithium-ion batteries *Electrochim. Acta* **212** 492–9
[10] Mohapatra S, Nair S V, Santhanagopalan D and Rai A K 2016 Nanoplate and mulberry-like porous shape of CuO as anode materials for secondary lithium ion battery *Electrochim. Acta* **206** 217–25

[11] Tao T *et al* 2011 MoO_3 nanoparticles dispersed uniformly in carbon matrix: a high capacity composite anode for li-ion batteries *J. Mater. Chem.* **21** 9350–5
[12] Du N *et al* 2007 Porous Co_3O_4 nanotubes derived from Co_4 (CO) 12 clusters on carbon nanotube templates: a highly efficient material for Li-battery applications *Adv. Mater.* **19** 4505–9
[13] Liao J, Xiao X, Higgins D, Lee D, Hassan F and Chen Z 2013 Hierarchical li 4 ti $5O_{12}$–TiO_2 composite microsphere consisting of nanocrystals for high power li-ion batteries *Electrochim. Acta* **108** 104–11
[14] Li W and Fu Z 2010 Nanostructured WO_3 thin film as a new anode material for lithium-ion batteries *Appl. Surf. Sci.* **256** 2447–52
[15] Du N *et al* 2007 Porous Co_3O_4 nanotubes derived from Co4 $(CO)_{12}$ clusters on carbon nanotube templates: a highly efficient material for Li-battery applications *Adv. Mater.* **19** 4505–9
[16] Park C, Kim J, Kim H and Sohn H 2010 Li-alloy based anode materials for li secondary batteries *Chem. Soc. Rev.* **39** 3115–41
[17] Zhang W 2011 A review of the electrochemical performance of alloy anodes for lithium-ion batteries *J. Power Sources* **196** 13–24
[18] Kim W, Hwa Y, Jeun J, Sohn H and Hong S 2013 Synthesis of SnO_2 nano hollow spheres and their size effects in lithium ion battery anode application *J. Power Sources* **225** 108–12
[19] Chang W, Park C, Kim J, Kim Y, Jeong G and Sohn H 2012 Quartz (SiO_2): a new energy storage anode material for li-ion batteries *Energy & Environmental Science.* **5** 6895–9
[20] Yin S, Song L, Wang X, Zhang M, Zhang K and Zhang Y 2009 Synthesis of spinel li 4 ti $5O_{12}$ anode material by a modified rheological phase reaction *Electrochim. Acta* **54** 5629–33
[21] Fehse M, Fischer F, Tessier C, Stievano L and Monconduit L 2013 Tailoring of phase composition and morphology of TiO_2-based electrode materials for lithium-ion batteries *J. Power Sources* **231** 23–8
[22] Eftekhari A 2017 Low voltage anode materials for lithium-ion batteries *Energy Storage Mater.* **7** 157–80
[23] Xu T, Wang W, Gordin M L, Wang D and Choi D 2010 Lithium-ion batteries for stationary energy storage *JOM Journal of the Minerals, Metals and Materials Society.* **62** 24–30
[24] Kebede M, Zheng H and Ozoemena K I 2016 Metal oxides and lithium alloys as anode materials for lithium-ion batteries *Nanomaterials in advanced batteries and supercapacitors.* (Berlin: Springer) 55–91
[25] Wen L, Luo H, Liu G and Zheng H 2016 Nanostructured lithium titanates (Li 4 Ti 5 O_{12}) for lithium-ion batteries *Nanomaterials In Advanced Batteries and Supercapacitors.* (Berlin: Springer) 127–69
[26] Ncube N M, Mhlongo W T, McCrindle R I and Zheng H 2018 The electrochemical effect of al-doping on $Li_4Ti_5O_{12}$ as anode material for lithium-ion batteries *Materials Today: Proceedings.* **5** 10592–601
[27] Medina P *et al* 2015 Li 4 ti $5O_{12}$/graphene nanoribbons composite as anodes for lithium ion batteries *SpringerPlus.* **4** 643
[28] Hu Y, Kienle L, Guo Y and Maier J 2006 High lithium electroactivity of nanometer-sized rutile TiO_2 *Adv. Mater.* **18** 1421–6
[29] Guan D, Cai C and Wang Y 2011 Amorphous and crystalline TiO_2 nanotube arrays for enhanced li-ion intercalation properties *J. Nanosci. Nanotechnol.* **11** 3641–50
[30] Rajeshwar K, Chenthamarakshan C, Goeringer S and Djukic M 2001 Titania-based heterogeneous photocatalysis. materials, mechanistic issues, and implications for environmental remediation *Pure Appl. Chem.* **73** 1849–60
[31] Primo A, Corma A and García H 2011 Titania supported gold nanoparticles as photocatalyst *Phys. Chem. Chem. Phys.* **13** 886–910
[32] Cai Y *et al* 2015 Hierarchically structured porous TiO_2 spheres constructed by interconnected nanorods as high performance anodes for lithium ion batteries *Chem. Eng. J.* **281** 844–51
[33] Wang Y, Su X and Lu S 2012 Shape-controlled synthesis of TiO_2 hollow structures and their application in lithium batteries *J. Mater. Chem.* **22** 1969–76
[34] Ren Y, Liu Z, Pourpoint F, Armstrong A R, Grey C P and Bruce P G 2012 Nanoparticulate TiO_2 (B): an anode for lithium-ion batteries *Angewandte Chemie.* **124** 2206–9
[35] Moretti A *et al* 2013 Investigation of different binding agents for nanocrystalline anatase TiO_2 anodes and its application in a novel, green lithium-ion battery *J. Power Sources* **221** 419–26
[36] Armstrong G, Armstrong A R, Bruce P G, Reale P and Scrosati B 2006 TiO_2 (B) nanowires as an improved anode material for lithium-ion batteries containing $LiFePO_4$ or $LiNi_0$. $5Mn_1$. $5O_4$ cathodes and a polymer electrolyte *Adv. Mater.* **18** 2597–600
[37] Mo L and Zheng H 2019 Growth of MnO_2 nanoflakes on TiO_2 nanorods for pseudocapacitor *J Alloys Compounds.* **788** 1162–8
[38] Machado N R F and Santana V S 2005 Influence of thermal treatment on the structure and photocatalytic activity of TiO_2 P25 *Catal. Today* **107** 595–601
[39] Yu J, Yu H, Cheng B and Trapalis C 2006 Effects of calcination temperature on the microstructures and photocatalytic activity of titanate nanotubes *J. Mol. Catal. A: Chem.* **249** 135–42
[40] Lan Y *et al* 2005 Titanate nanotubes and nanorods prepared from rutile powder *Adv. Funct. Mater.* **15** 1310–8
[41] Liu N, Chen X, Zhang J and Schwank J W 2014 A review on TiO_2-based nanotubes synthesized via hydrothermal method: formation mechanism, structure modification, and photocatalytic applications *Catal. Today* **225** 34–51
[42] Luan X and Wang Y 2014 Thermal annealing and graphene modification of exfoliated hydrogen titanate nanosheets for enhanced lithium-ion intercalation properties *Journal of Materials Science & Technology.* **30** 839–46
[43] Zhang Z *et al* 2014 Flower-like hydrogenated TiO_2 (B) nanostructures as anode materials for high-performance lithium ion batteries *J. Power Sources* **267** 388–93
[44] Liu H *et al* 2011 Mesoporous TiO_2–B microspheres with superior rate performance for lithium ion batteries *Adv. Mater.* **23** 3450–4
[45] Liu S *et al* 2013 A flexible TiO_2 (B)-based battery electrode with superior power rate and ultralong cycle life *Adv. Mater.* **25** 3462–7
[46] Wu D *et al* 2016 Simple synthesis of TiO_2/MnOx composite with enhanced performances as anode materials for li-ion battery *Electrochim. Acta* **211** 832–41